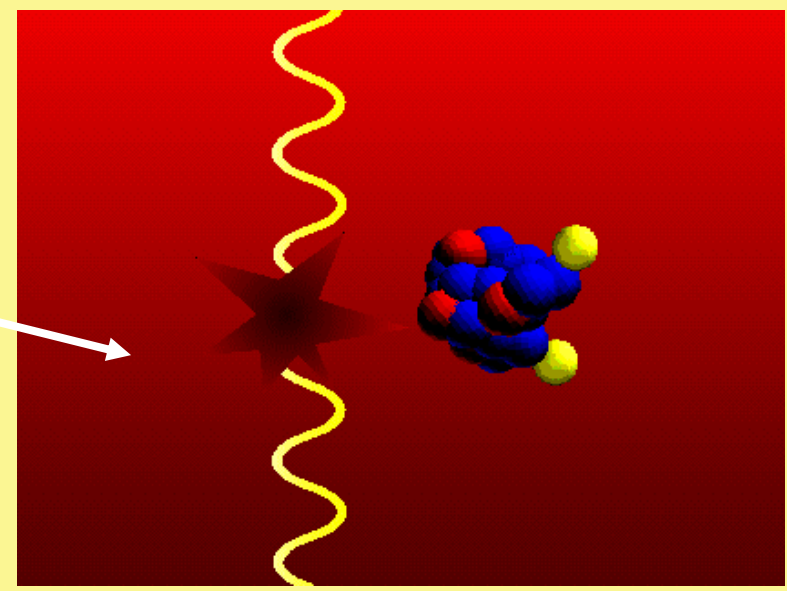
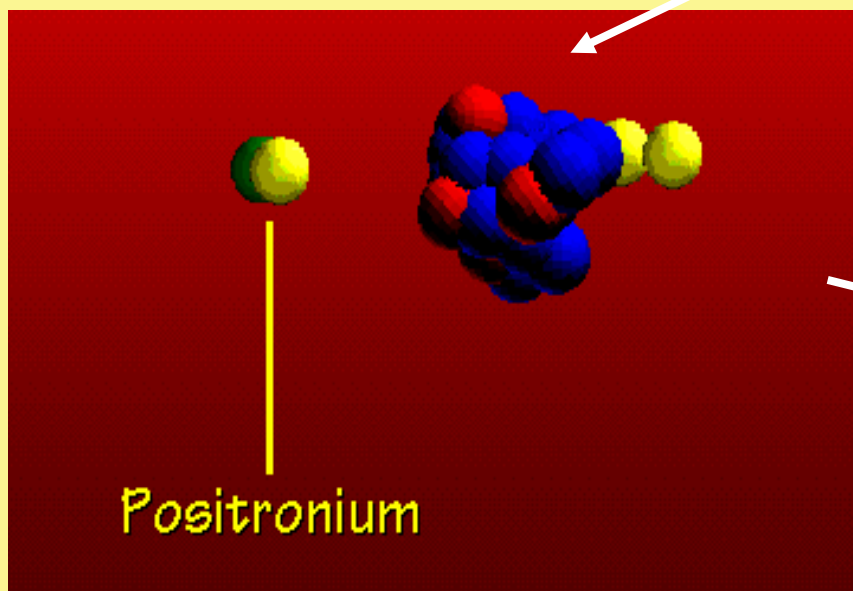
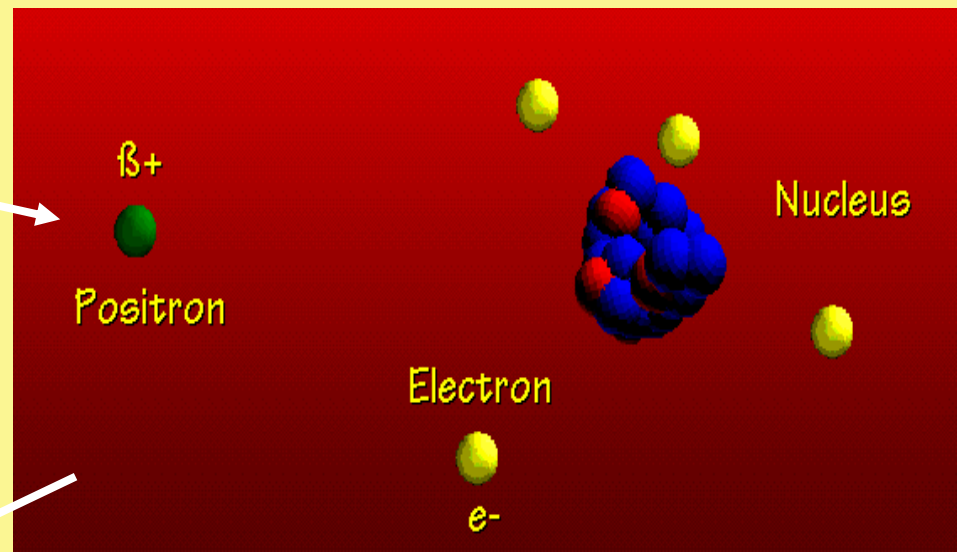
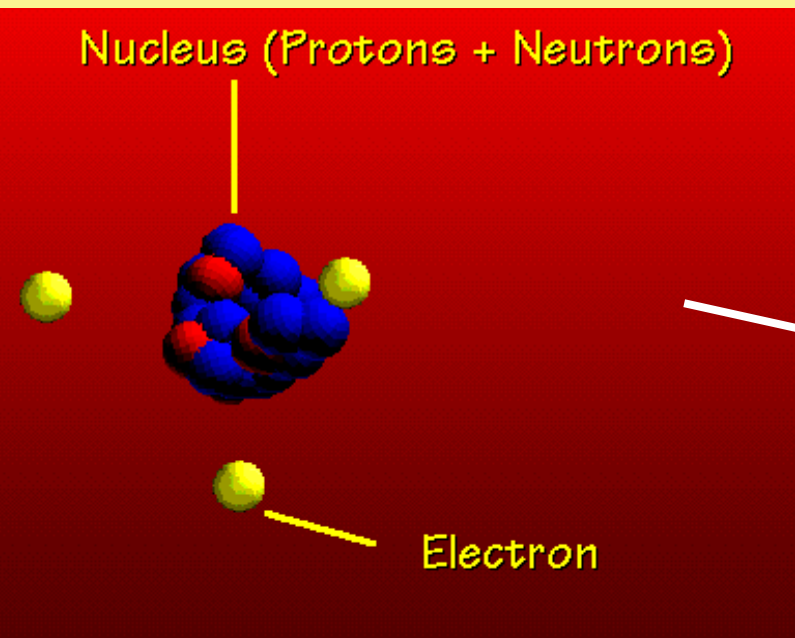


# CANOA 2017

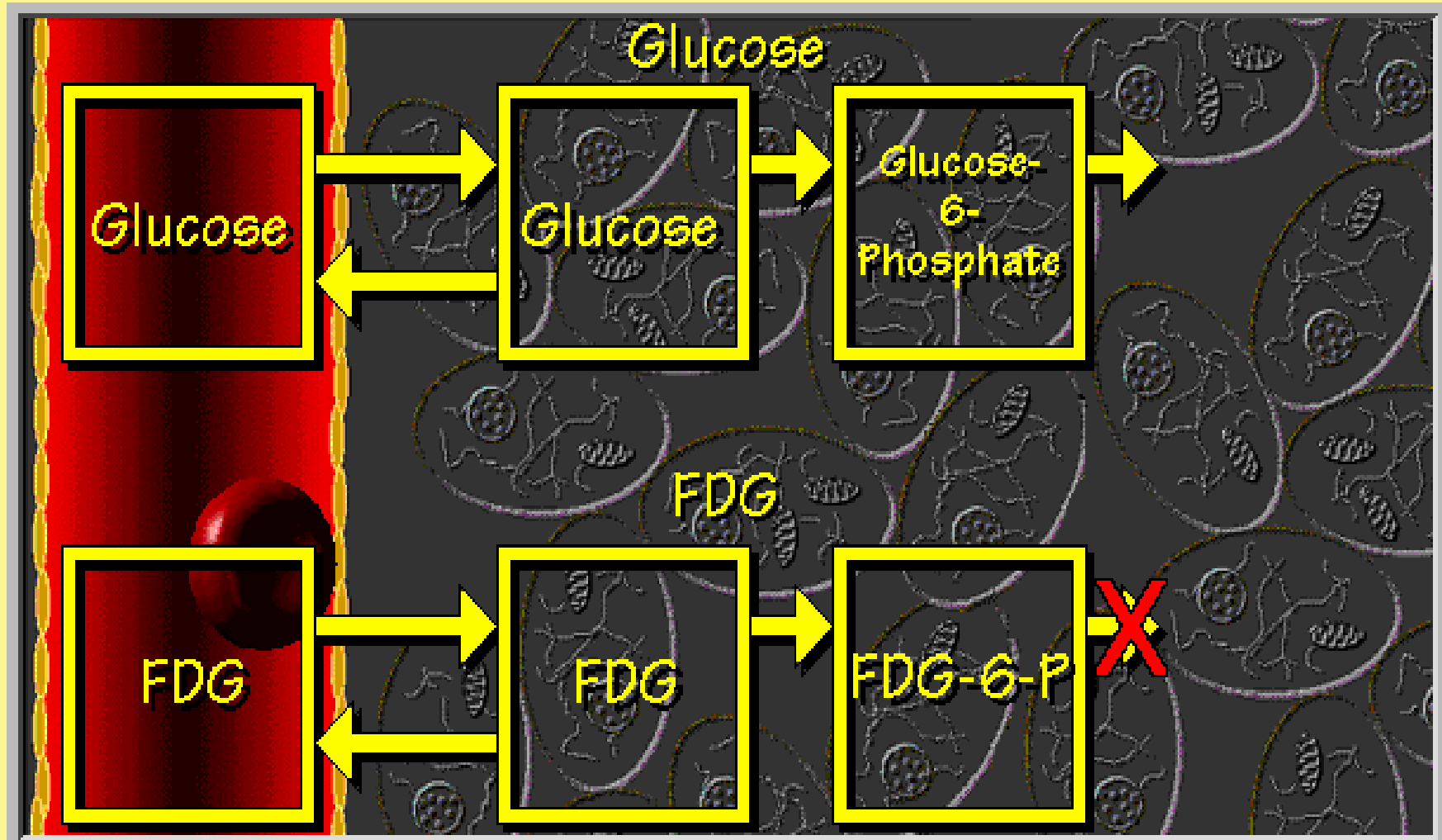
## Breast cancer and immuno....PET

**Dr. Matteo Salgarello**  
Servizio di Medicina Nucleare, Centro PET, Ospedale Sacrocuore-Don Calabria, Negrar, VR.  
[matteo.salgarello@sacrocuore.it](mailto:matteo.salgarello@sacrocuore.it), tel 045/6014611

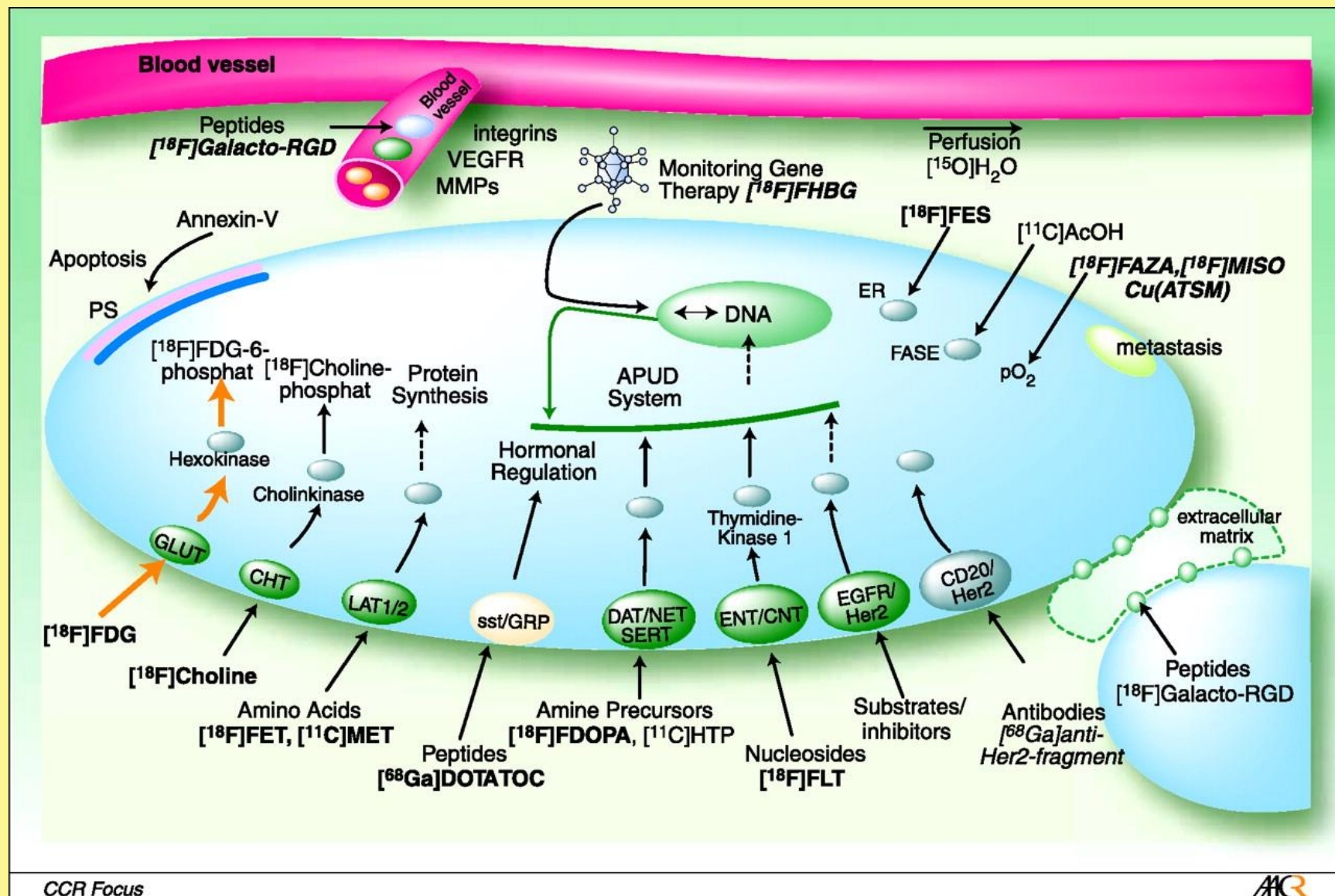
# Annichilazione del positrone



L' FDG iniettato al paziente agisce come tracciante della glicolisi e si accumula maggiormente in sedi ove questa via metabolica è attivata in misura abnorme rispetto al consueto metabolismo aerobico, cosa che avviene in varie condizioni patologiche, come ad esempio nel contesto di tumori primitivi e di loro metastasi.



# Selected targets and corresponding nuclear imaging probes already established for nuclear molecular imaging in the clinic or currently under assessment in clinical studies



CCR Focus



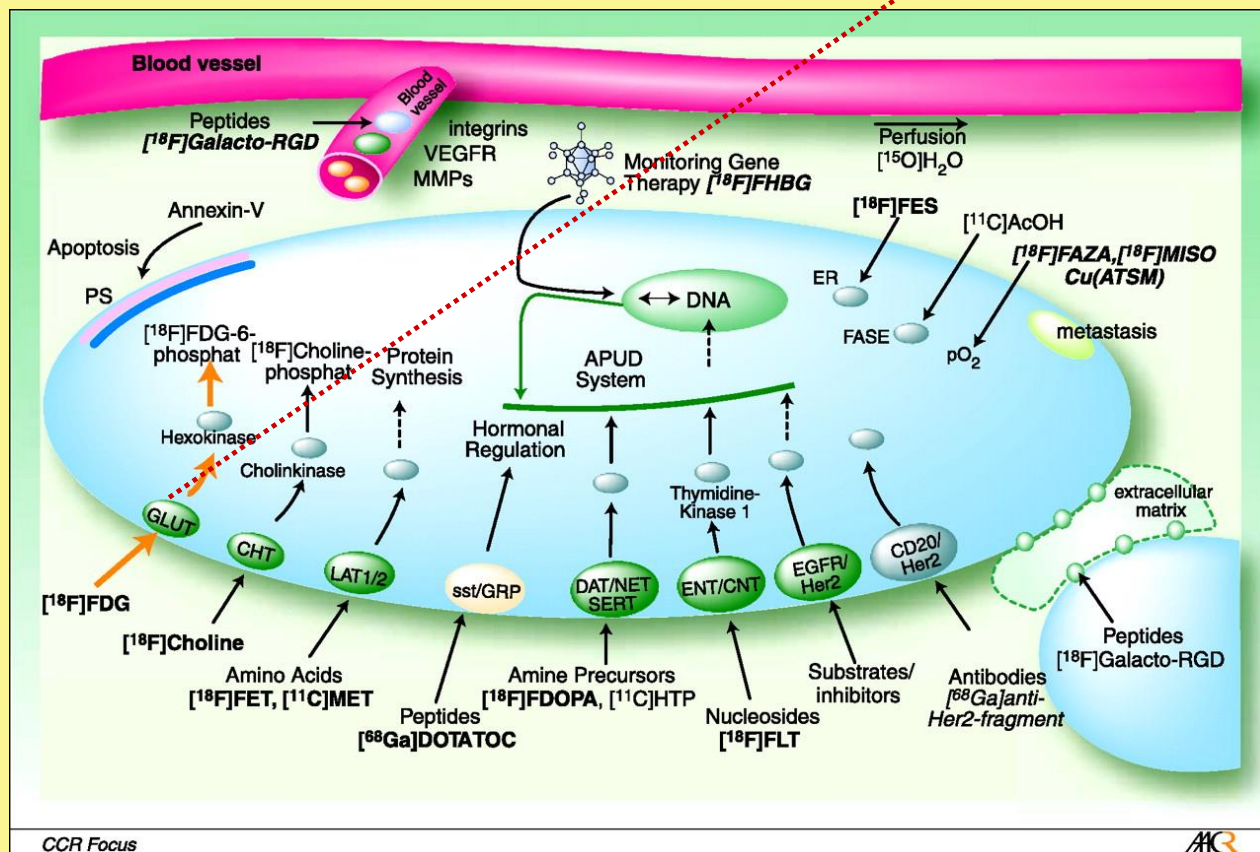
Wester H Clin Cancer Res 2007;13:3470-3481



Clinical Cancer Research

# Selected targets and corresponding nuclear imaging probes already established for nuclear molecular imaging in the clinic or currently under assessment in clinical studies

E' veramente l'unica  
informazione  
oncologicamente rilevante?



Wester H Clin Cancer Res 2007;13:3470-3481

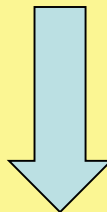


# Breast Cancer and Micad

## Molecular Imaging Contrast Agent Database

- 1: [Human Studies](#): PET18F -> 16 $\alpha$ -[18F]Fluoro-17 $\beta$ -estradiol
  - 2: [Background](#): PET64Cu -> HSDAVFTDNYTKLRKQ-Nle-AVKK-(3-OCH3,4-OH)-FLNSSV-GABA-L-(Dap-(BMA)2)-64Cu
  - 3: [Background](#): Multimodal64Cu, quantum dot (QD705) -> 64Cu-1,4,7,10-Tetraazacyclododecane-1,4,7,10-tetraacetic acid-quantum dot-vascular endothelial growth factor
  - 4: [Background](#): PET64Cu -> 64Cu-DOTA hu4D5v8 (scFv-CH2-CH3)2
  - 5: [Human Studies](#): PET18F -> [18F]Fluorocholine
  - 6: [Background](#): PET64Cu -> 64Cu-N,N'-Bis(S-benzoyl-thioglycolyl)diaminopropanoate-KRAS-PNA-d(Cys-Ser-Lys-Cys)
  - 7: [Human Studies](#): PET18F -> 3'-Deoxy-3'-[18F]fluorothymidine
  - 8: [Rodents](#): PET18F -> 16 $\alpha$ -[18F]Fluoro-17 $\beta$ -estradiol -> Animal Studies
  - 9: [Background](#): SPECT99mTc -> 99mTc-N,N'-Bis(S-benzoyl-thioglycolyl)diamidopropenoyl-KRAS-PNA-d(Cys-Ser-Lys-Cys)
  - 10: [Human Studies](#): PET18F -> [18F]Fluoro-2-deoxy-2-D-glucose
  - 11: [Rodents](#): PET64Cu -> 64Cu-1,4,7,10-Tetraazacyclododecane-N,N',N'',N'''-tetraacetic acid-interleukin-18-binding protein-Fc -> Animal Studies
  - 12: [Rodents](#): PET68Ga -> 68Ga-Trastuzumab F(ab') fragment -> Animal Studies
  - 13: [Background](#): PET11C -> I-[methyl-11C]Methionine
  - 14: [Background](#): SPECT99mTc -> 99mTc-glutamate peptide 3-aminoethyl estradiol
  - 15: [Background](#): PET18F -> 5-[(E)-2-(4-[18F]Fluorophenyl)ethenyl]-1,3-benzenediol
  - 16: [Background](#): PET89Zr -> 89Zr-Labeled trastuzumab, a humanized monoclonal antibody against epidermal growth factor receptor 2
  - 17: [Background](#): PET64Cu -> 64Cu-1,4,7-Triazacyclononane-1,4-diacetate-8-aminoctanoic acid-Gln-Trp-Ala-Val-Gly-His-Leu-Met-NH2
  - 18: [Background](#): PET11C -> [O-11C-methyl]4-N-(3-Bromoanilino)-6,7-dimethoxyquinazoline
  - 19: [Background](#): PET11C -> (S)-6-[(4-Chlorophenyl)(1H-1,2,4-triazol-1-yl)methyl]-1-[11C]methyl-1H-benzotriazole
  - 20: [Background](#): PET64Cu -> 64Cu-1,4,7,10-Tetraazacyclododecane-N,N',N'',N'''-tetraacetic acid-interleukin-18-binding protein-Fc
  - 21: [Rodents](#): PET64Cu -> 64Cu-DOTA hu4D5v8 (scFv-CH2-CH3)2 -> Animal Studies
  - 22: [Background](#): PET18F -> [18F]Fluoro-2-deoxy-2-D-glucose
  - 23: [Rodents](#): PET11C -> N-[N-[(S)-1,3-Dicarboxypropyl]carbamoyl]-S-[11C]methyl-L-cysteine -> Animal Studies
  - 24: [Rodent an humans](#): PET11C -> [11C]Choline -> Animal Studies
  - 25: [Human Studies](#): PET18F -> 1-(2'-Deoxy-2'-[18F]-fluoro- $\beta$ -D-arabinofuranosyl)thymine
- NB) Possibilità di utilizzo del Na-18F, per la ricerca di metastasi ossee o per studi MIXED con FDG.

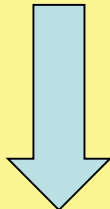
# CANOA 2017



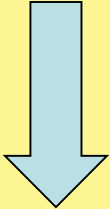
**Fare la Pet?...Quando la PET?...Quale PET?**



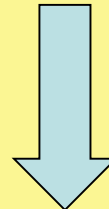
Diagnosi  
iniziale



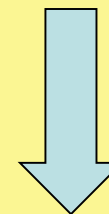
Prognosi



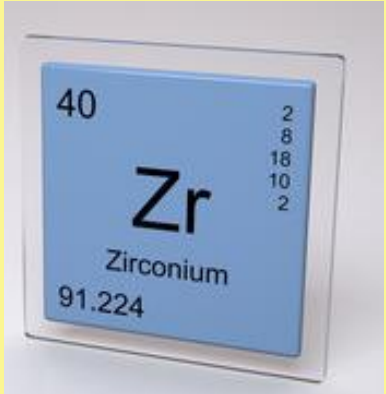
Ristadiazione



Monitoraggio della risposta a  
trattamento



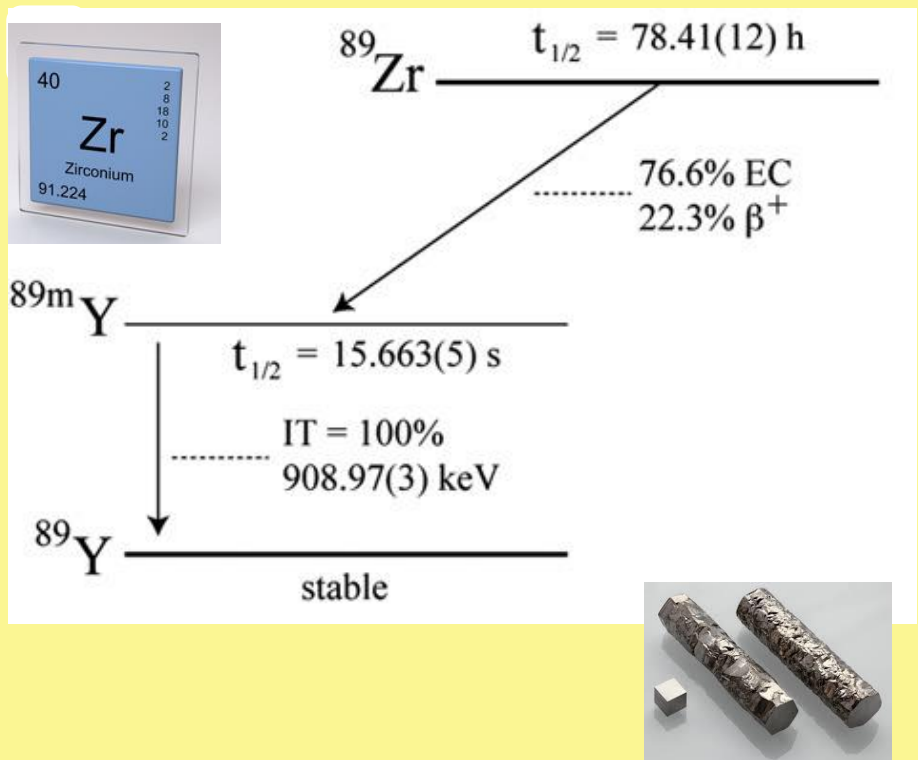
Follow-up



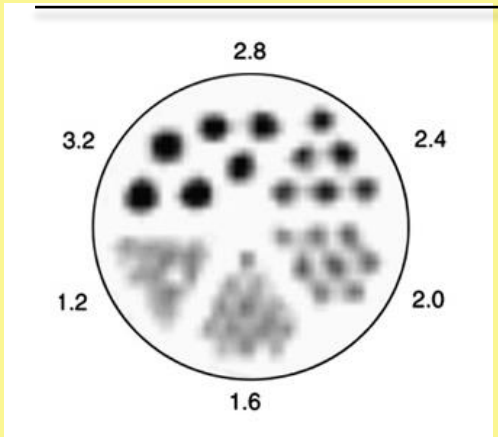
# Nuova Agenda di lavoro

- $^{89}\text{Zr}$  Nuclear Properties, Production
- $^{89}\text{Zr}$  Chemistry a Labelling
- $^{89}\text{Zr}$  Application

# Zirconium-89 [ $^{89}\text{Zr}$ ]



Half-life	78.4 h
Decay Mode	$\epsilon = 76.6\%$ $\beta^+ = 22.3\%$
$E(\beta^+)$	395.5 kev
$E(\gamma)$	511 KeV 909.2 Kev
$R_{ave} (\beta^+)$	1.2 mm

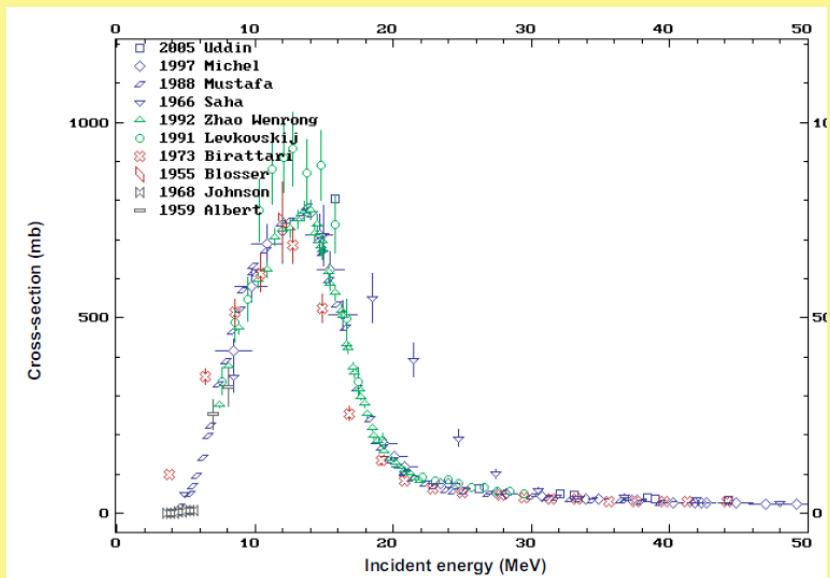


# Nuclear reaction for $^{89}\text{Zr}$ production

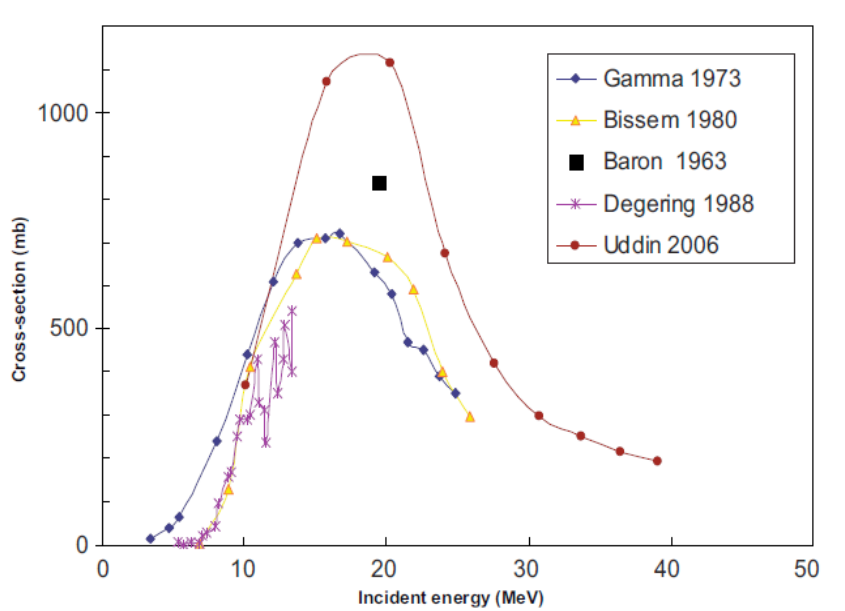
$^{89}\text{Y}(\text{p},\text{n})^{89}\text{Zr}$

$^{89}\text{Y}(\text{d},2\text{n})^{89}\text{Zr}$

$\text{nat Sr}(\alpha,\text{xn})^{89}\text{Zr}$



Excitation function for  $^{89}\text{Y}(\text{d},2\text{n})^{89}\text{Zr}$  reaction

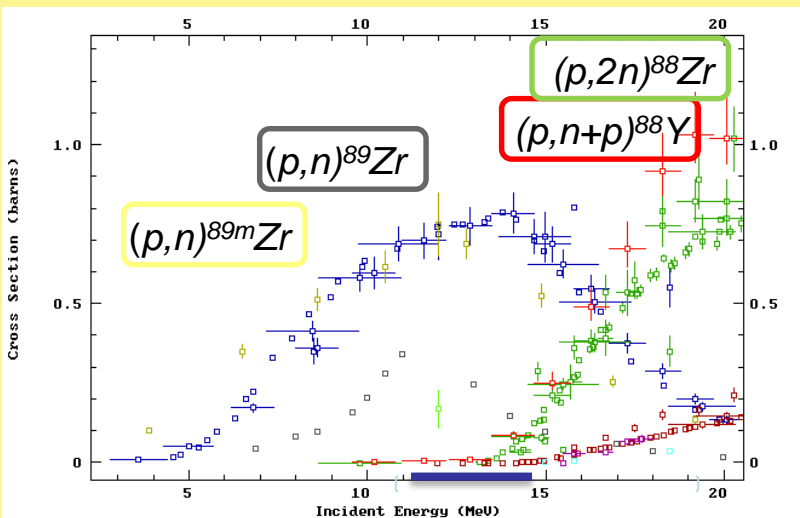


Excitation function for  $^{89}\text{Y}(\text{p},\text{n})^{89}\text{Zr}$  reaction

# $^{89}\text{Zr}$ with medical cyclotron



$^{89}\text{Y}(\text{p},\text{n})^{89}\text{Zr}$



## Competitive Nuclear Reaction:

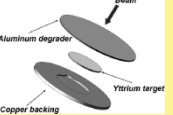
$^{89}\text{Y}(\text{p},\text{n})^{89m}\text{Zr}$  (>3.8 MeV, 4.2 m)

$^{89}\text{Y}(\text{p},2\text{n})^{88}\text{Zr}$  (>13.076 MeV, 83.4 d)

$^{89}\text{Y}(\text{p},\text{pn})^{88}\text{Y}$  (>11.609 MeV, 106.6 d)



# Target for $^{89}\text{Zr}$ production

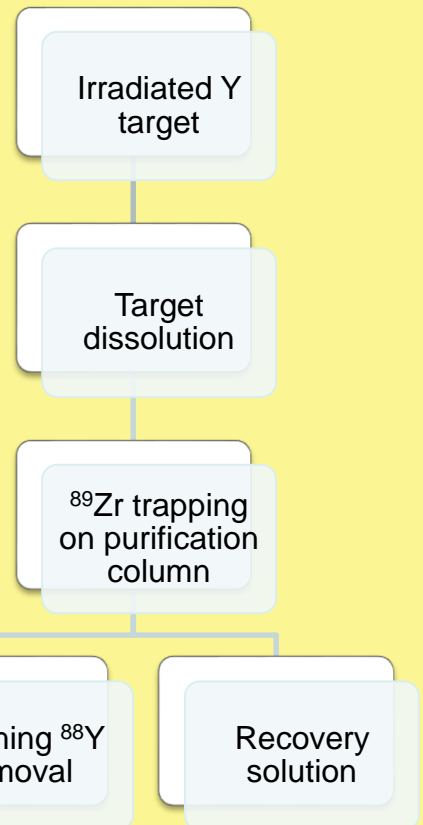
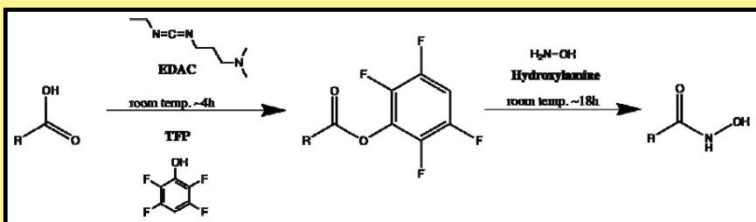
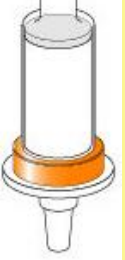
		Beam Energy (MeV)	Y foil thickness (mm)	Beam parameter	Yield (MBq/ $\mu\text{Ah}$ )	Radionuclidian Purity		
DeGrado*	2016	14	2M $\text{Y}(\text{NO}_3)_3$	2h@40 $\mu\text{A}$	4.4	99%		Mayo Clinic
Wooten	2013	14.7	0.64	4h@15 $\mu\text{A}$	55.5	99.998%		Washington University
Cicoria	2011	12.6	0.30	1h@20 $\mu\text{A}$	70.5	99.9995%		S.Orsola Hospital
Holland	2005	15	0.10	5h@15 $\mu\text{A}$	55	99.9%		Memorial Sloan Kettering Center
Verel	2003	14	0.035 sputtered	1h@20 $\mu\text{A}$	80.5	99.99%		Negrar Hospital
Kandil	2007	12.6	13 ( $\text{Y}_2\text{O}_3$ )	5h@2 $\mu\text{A}$	27.9	99.9%		Julich Center

# $^{89}\text{Zr}$ Recovery

Negar EZAG module used for processing  
Target material and riformulation of  $^{89}\text{Zr}$ solution

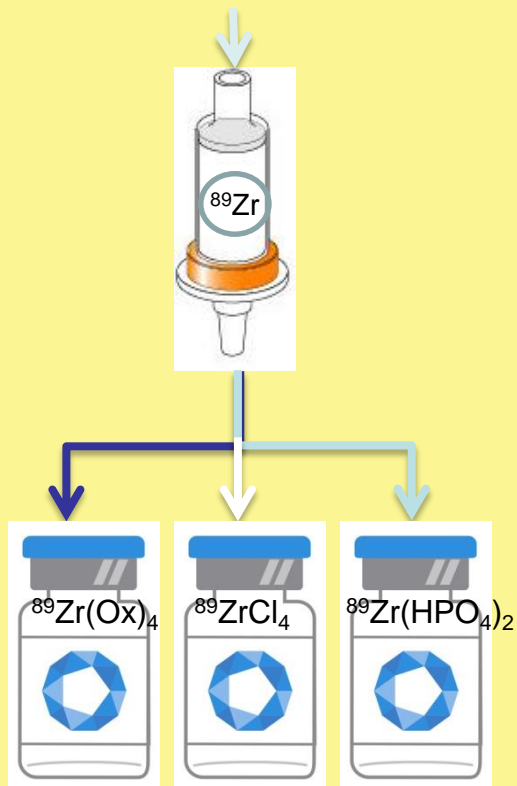


Cation exchange  
resin  
funzionalized to  
hydroxamic groups



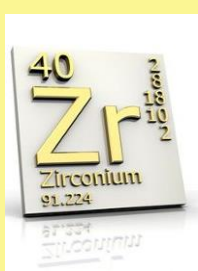
# $^{89}\text{Zr}$ Formulation

HOX 1M / HCl 1M /PBS 1.2 M



- **Oxalic** in large amounts can lead to decalcification of blood and acute kidney failure, by precipitation of solid Ca. EMA ( tox Ox 25 mg/Kg).
- The **Oxalic** concentration ( usually 1M) are **close to saturation** (1.1 M) than it will be difficult to evaporate or reconstitute in a more concentrate solution.
- **Cloridric** precursor, **no standard procedure** to labelling Antibody are available.
- Cloridric, **need to be removed** before Mab labelling.
- **PBS ideal** for labelling Antibody.
- **Low recovery 80%.**
- **All the eluent solution** need to be evaluated by SA and **ICPMass** to minimize the metal contaminants.

# $^{89}\text{Zr}$ Coordination Chemistry



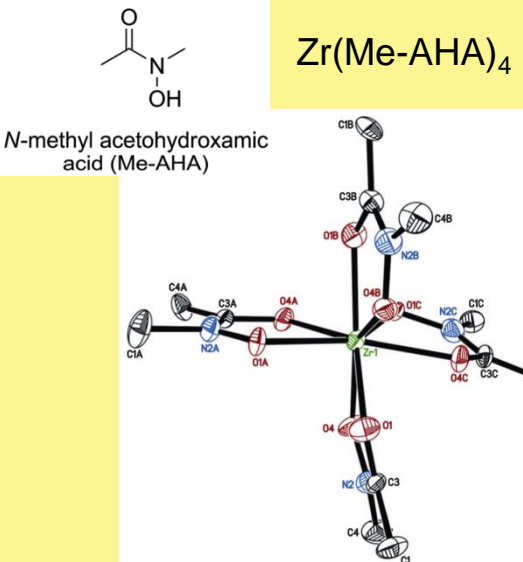
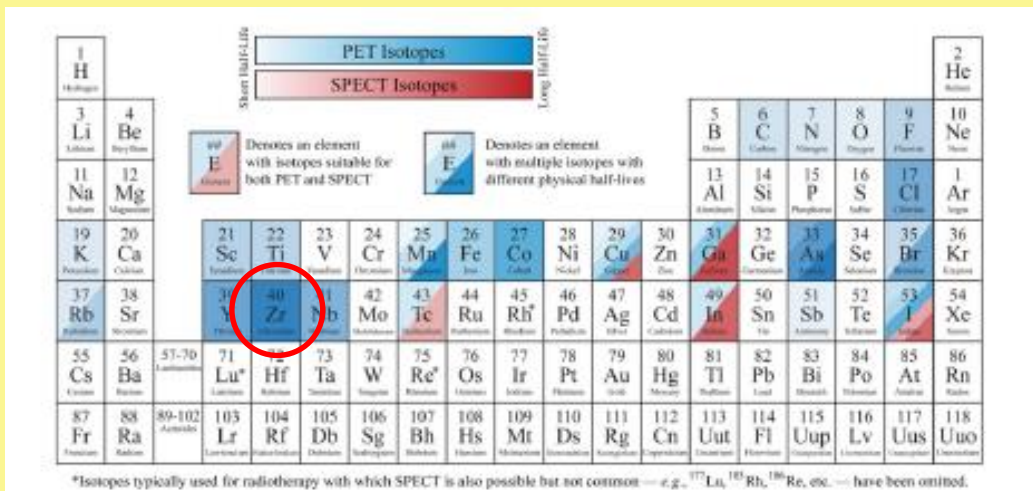
Zr is a IV group metal.

Zr exist on water solution on  $\text{Zr}^{4+}$ .

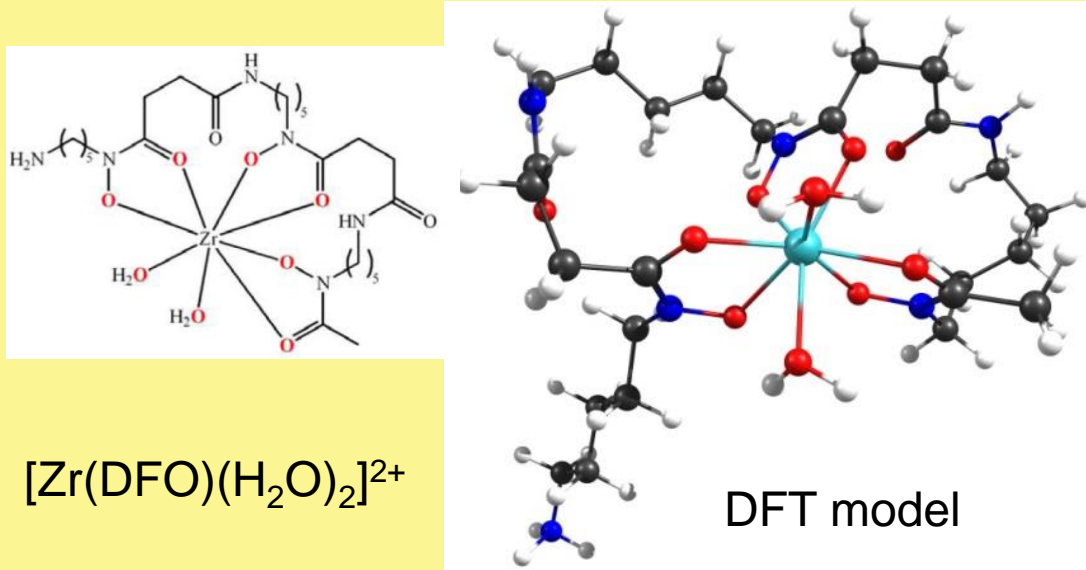
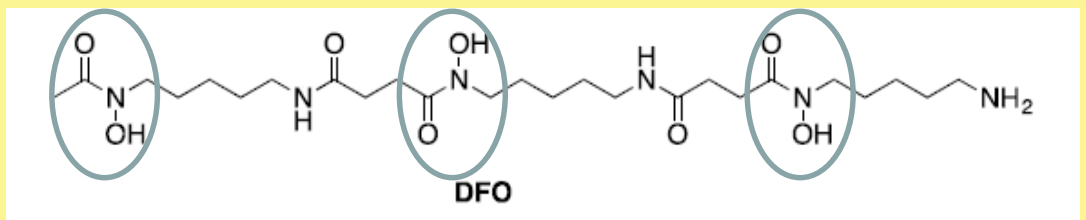
Cation relatively large , highly charged ion “Hard ion”

Complexes with **high coordination numbers**

Prefer Ligands wit **Oxygen donors** ( charged or not)

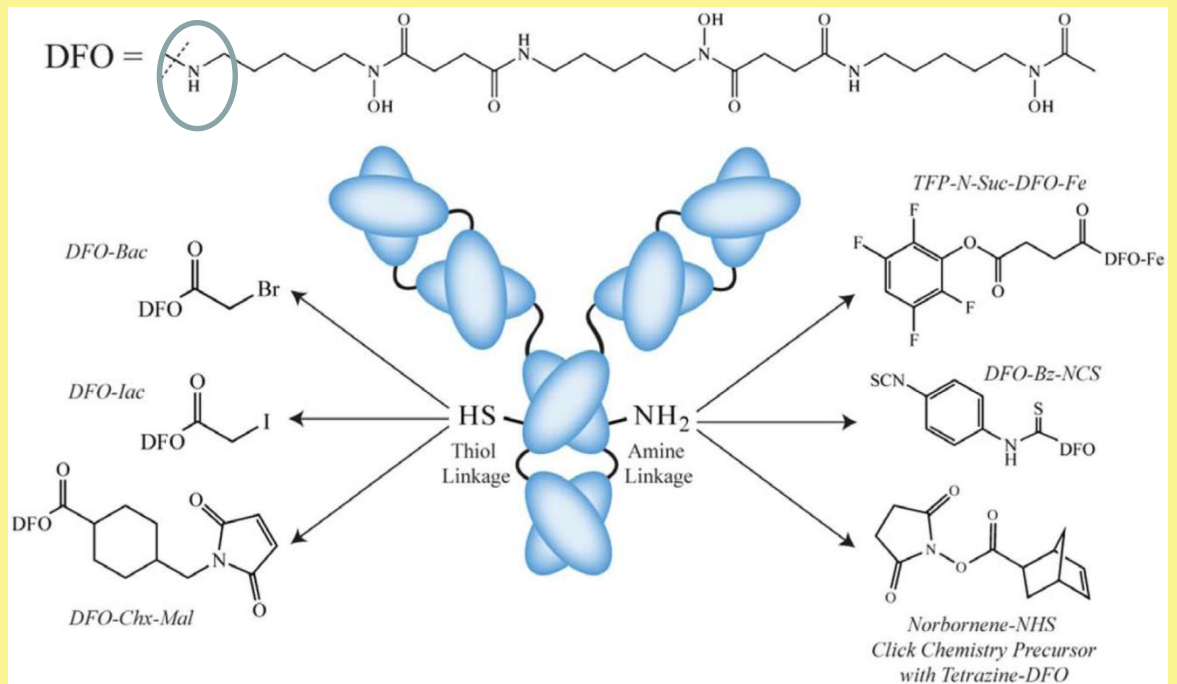


# Desferrioxamine B (DFO)



DFO is a chelant which contains hydroxamate groups hexadentate three anion chelator. Deprotonation of hydroxy groups results in hexadentate ligand. Are naturally created from Streptomyces bacteria. FDA approved DFO like a drug for acute iron intoxication. Make less concerns if it will be dissociated from mAb.

# DFO Conjugation

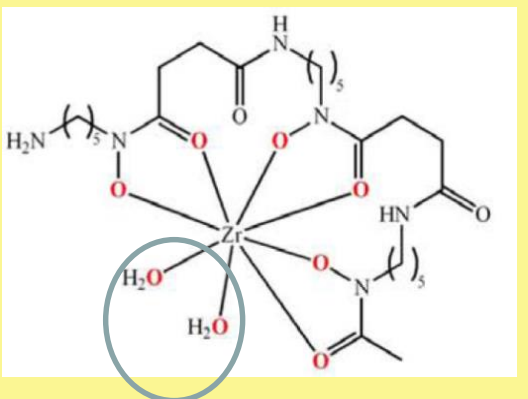
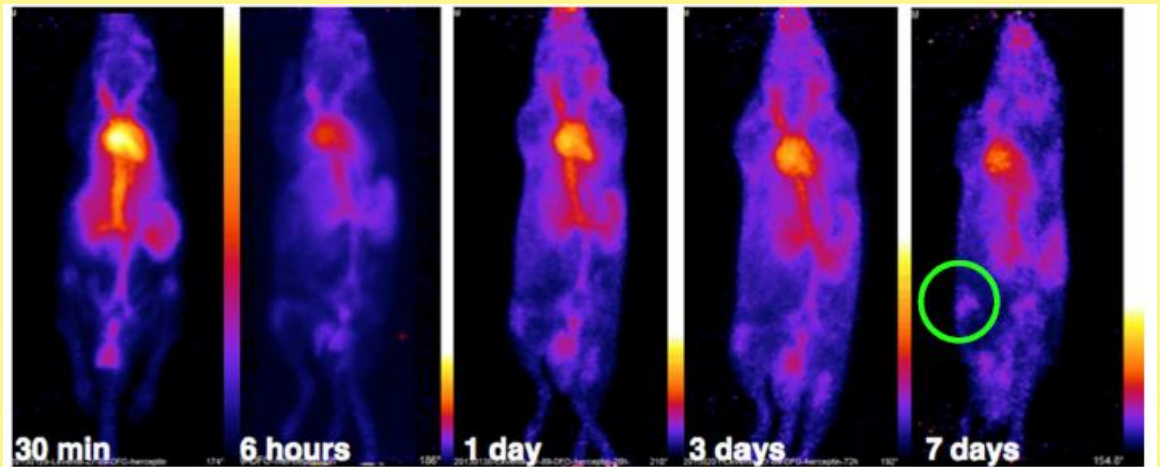


- DFO present a primary amino group can be functionalized.
- The modify DFO can be used to linkage Thiol goup or Amine goups present on biological molecules.

Typical reaction condition:

- DMSO solvent
- 3-10 fold excess of ligand
- 30-37 °C
- PD10 purification

# DFO Stability

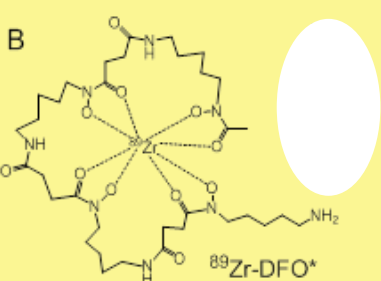
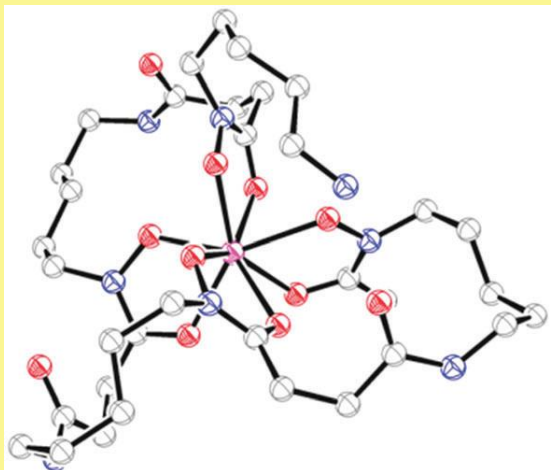
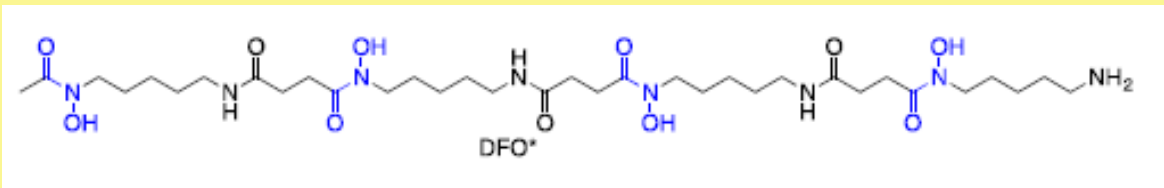


$[^{89}\text{Zr}]\text{ZrDFOTрастузумаб}$

$^{89}\text{Zr}^{4+}$  high bone affinity.  
 $^{89}\text{Zr}$  can be also accumulated on liver and spleen due to the colloidal form.

Water molecule in Zr coordination sphere lower the complex stability.  
 $\text{Zr}^{4+}$  ions prefer to be fully O<sup>6</sup>h structure in single coordination sphere.

# DFO\*

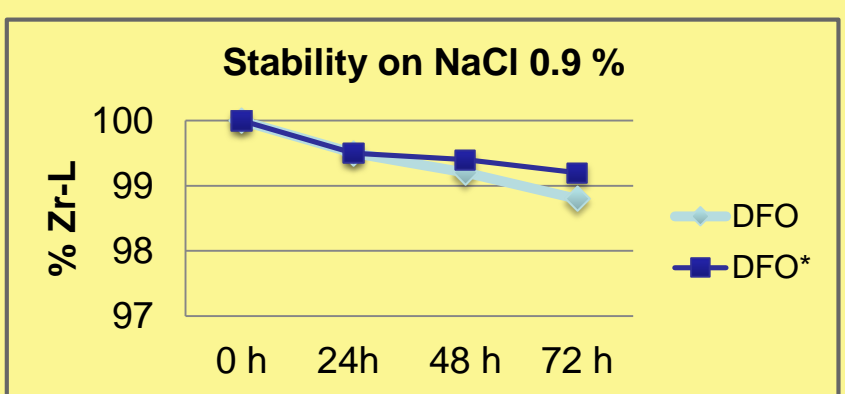


DFO\* is a chelant which contains four hydroxamate groups for Octadentate geometry.

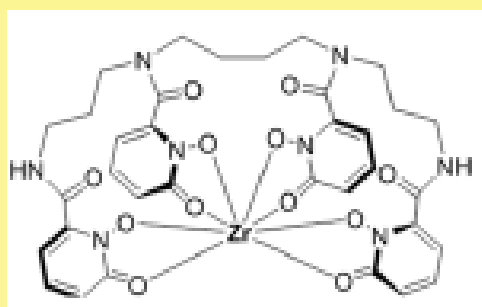
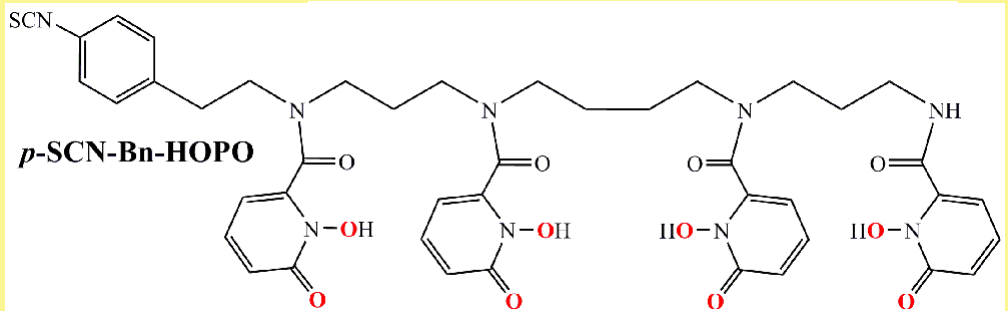
Deprotonation of hydroxy groups results in four anion ligand.

Similar reactivity of DFO.

DFT model



# HOPO Ligand



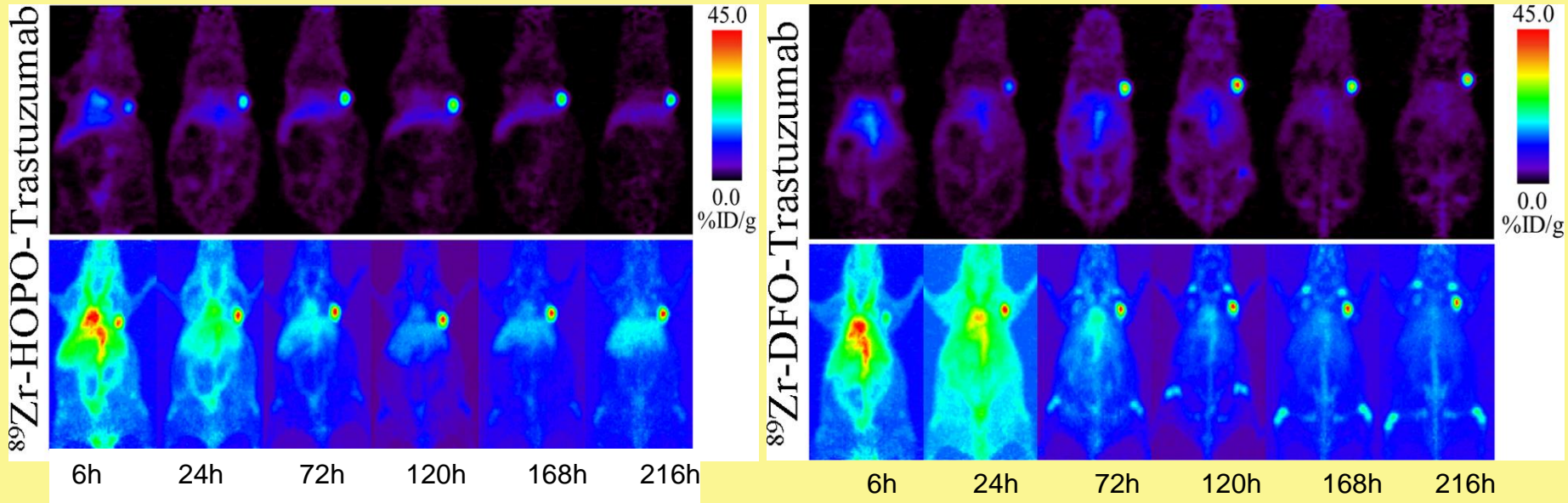
Crystal structure

HOPO is a Octadentate chelator with hydroxypyridinone groups ligand for metal binding Zr<sup>4+</sup> ion.

HOPO comes from Actinide sequestration literature, was studied for Pu<sup>4+</sup> stable complex.

HOPO present four hydroxypyridone groups with hard oxygen donors, appropriate for Zr<sup>4+</sup> binding.

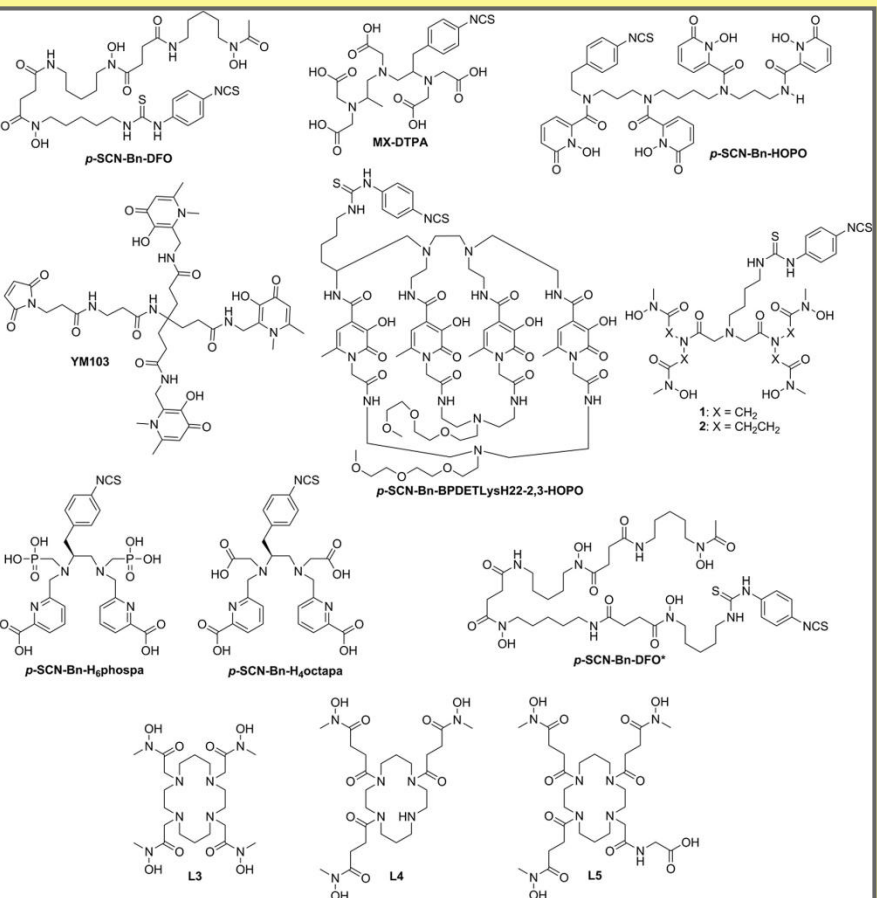
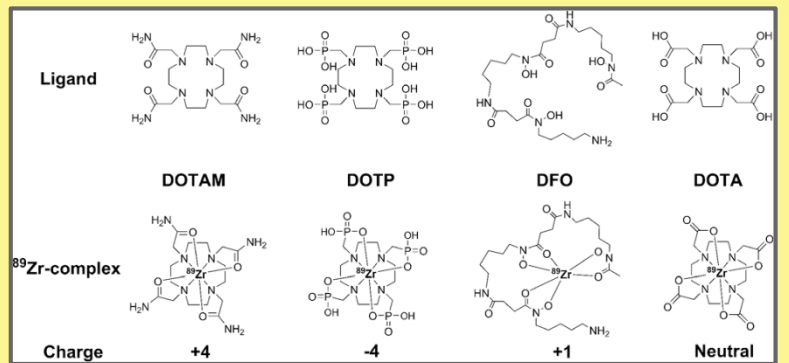
# HOPO Stability



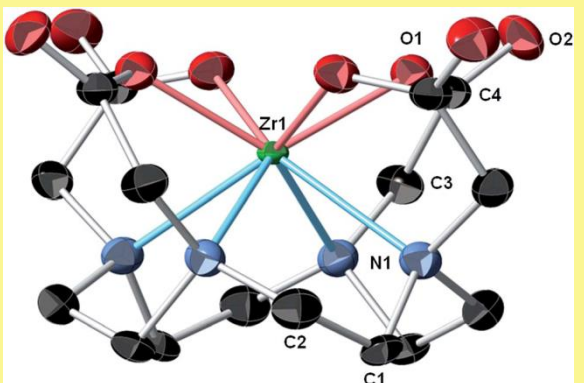
MicroPET images of  $^{89}\text{Zr}$ -HOPO-Trastuzumab and  $^{89}\text{Zr}$ -DFO-Trastuzumab in female athymic nude mice with BT474 xenografts on right shoulders inj (9.25-9.99 MBq) in 200  $\mu\text{L}$  0.9 %of sterile saline.

Both compounds show good tumor to background contrast, but  $^{89}\text{Zr}$ -DFO-Trastuzumab shows evidence of bone uptake suggestiong in vivo release of  $^{89}\text{Zr}^{4+}$

# Next generation ligands

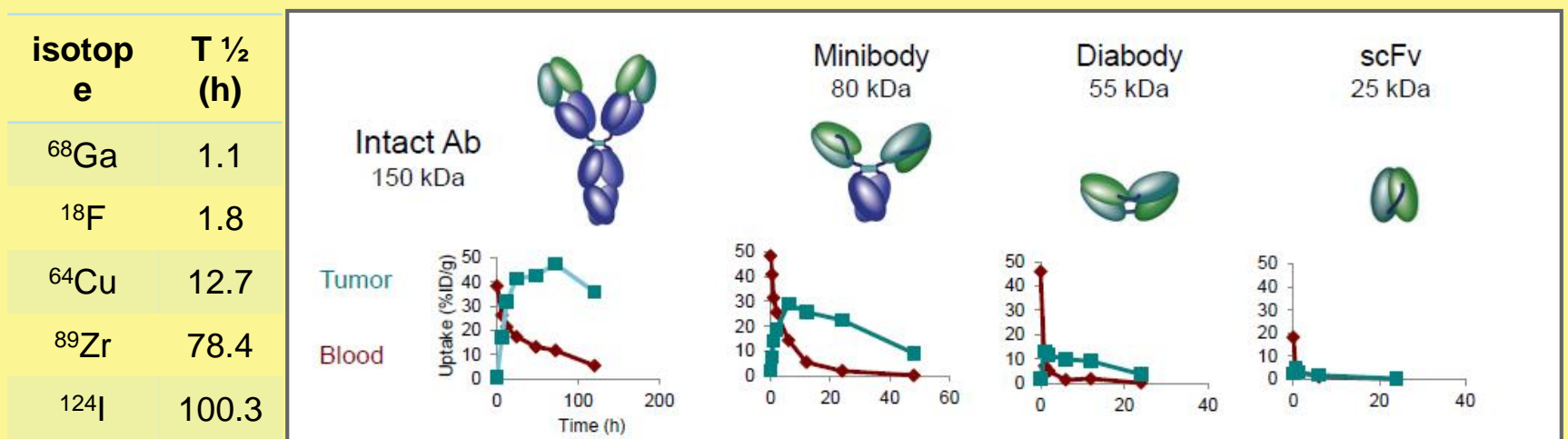


Back to the future



Crystal structure  
ZrDOTA

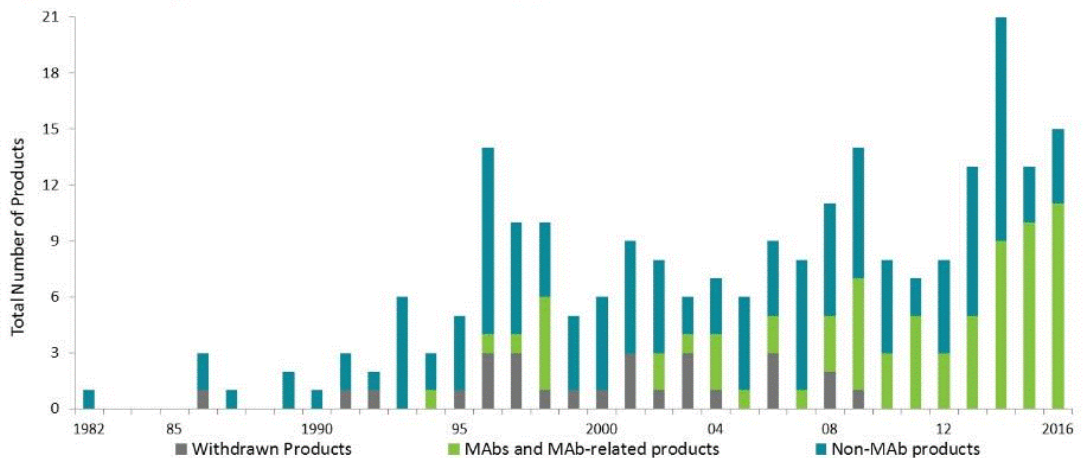
# Why we need $^{89}\text{Zr}$ ?



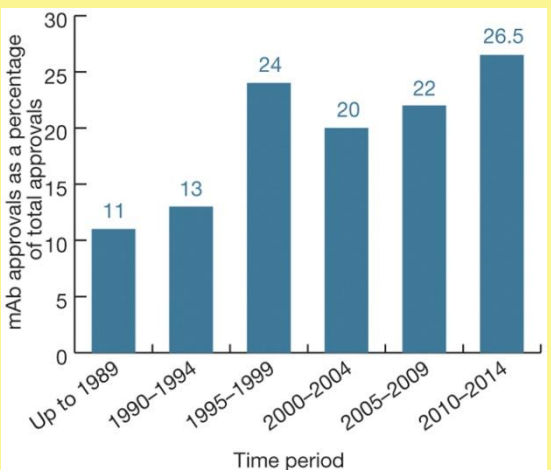
- Ideal for labelling compounds with long blood circulation times.
- Low positron emission energy provides better spatial resolution compared to other non standards isotopes ( $^{124}\text{I}$ ,  $^{68}\text{Ga}$ )
- Pub med 180 papers on  $^{89}\text{Zr}$  and in the last 5 years 124 articles majority of them related to Antibody labelling on immunoPET field.

# Biopharmaceutical

Figure 1. Biopharmaceutical Annual Approvals 1982-2016



The graph displays the number of products first approved for commercial sale in the US or Europe each year since 1982. Products approved but subsequently removed from the market are denoted in grey; MAb and MAB-related products are shown in green; non-MAb recombinant products are shown in blue. For 2016, the figure includes the number of products approved as of December 22.



Exponential approval in last 5 years.

Not only for Oncology.

Lot of focus on neurodegenerative pathology.

ImmunoPET potential help on  
drug approval studies.

# <sup>89</sup>Zr on pre-clinic

	Targeting Moiety	Target	Type of cancer	Conjugation Method
Antibodies	Cetuximab	EGFR	Multiple	N-suc-DFO
	Bevacizumab	VEGF	Head and neck squamous cell carcinoma; ovarian; breast	N-suc-DFO
	Trastuzumab	HER2	Breast; ovarian	N-suc-DFO
	J591	PSMA	Prostate	N-suc-DFO
	cmAb U36	CD44v6	Head and neck squamous cell carcinoma	N-suc-DFO
	5A10	fPSA	Prostate	N-suc-DFO
	cG250	MN/CA IX	Renal cell carcinoma	N-suc-DFO
	R1507	IGF-1R	Triple-negative breast	N-suc-DFO
	Fresolimumab	TGF- $\beta$	Multiple	N-suc-DFO
	DN30	Met	Gastric; head and neck squamous cell carcinoma	N-suc-DFO
	7E11	PSMA	Prostate	N-suc-DFO
	hRS7	EGP-1	Prostate	N-suc-DFO
	Panitumumab	HER1	Colorectal	DFO-Bz-NCS
	TRC105	CD105	Breast	DFO-Bz-NCS
Antibody fragments	Anti-B220	B cells	Unspecified	DFO-Bz-NCS
	E48 and 323/A3	Unspecified surface antigens	Head and neck squamous cell carcinoma; ovarian	SATA/SMCC thioether
	(aHGF)-Nanobodies	HGF	Glioma	DFO-Bz-NCS
	Ranibizumab (Fab)	VEGF-A isoforms	Ovarian	N-suc-DFO
	cG250-F(ab9)2	CAIX	Head and neck squamous cell carcinoma	N-suc-DFO
Peptides Nanomaterials	c(RGDfK) with and w/o PEG	Integrin $\alpha v \beta 3$	Breast	DFO-Bz-NCS
	Albumin	n/a	Prostate	N-suc-DFO
	Resin microspheres and SIR-Spheres	n/a	Liver	n/a
	Nanocolloidal albumin	n/a	Head and neck squamous cell carcinoma	DFO-Bz-NCS
	Dextran nanoparticles	Macrophages	Colon	DFO-Bz-NCS
	Single wall carbon nanotubes	VE-cad based on attached antibody E4G10	Colon adenocarcinoma	N-suc-DFO

16 Antibodies already labelled.

Multiple districts addressed.

Interesting nanoparticle application.

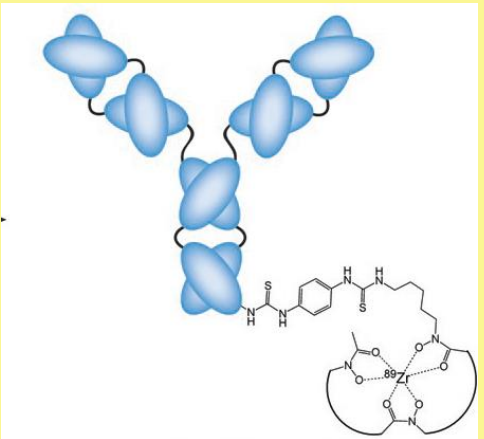
Only DFO chelating used.

# <sup>89</sup>Zr on clinic

**TABLE 1 | Summary of clinical studies on <sup>89</sup>Zr-immuno-PET in oncology.**

Author	Year	Target	mAb	Tumor type	N
Börjesson	2006	CD44v6	cmAb U36	Head and neck cancer	20
	2009				
Dijkers	2010	HER2	trastuzumab	Breast cancer	14
Rizvi	2012	CD20	ibritumomab-tiuxetan	B-cell lymphoma	7
Gaykema	2013	VEGF-A	bevacizumab	Breast cancer	23
van Zanten	2013	VEGF-A	bevacizumab	Glioma	3
van Asselt	2014	VEGF-A	bevacizumab	Neuroendocrine tumors	14
Bahce	2014	VEGF-A	bevacizumab	Non-small cell lung cancer	7
Pandit-Taskar	2014	PSMA	Hu-J591	Prostate cancer	50
	2015				
Den Hollander	2015	TGF-β	fresolimumab	Glioma	12
Gaykema	2015	HER2	trastuzumab	Breast cancer	10
		VEGF-A	bevacizumab		6
Gebhart	2015	HER2	trastuzumab	Breast cancer	56
Lamberts	2015	MSLN	MMOT0530A	Pancreatic cancer	11
				Ovarian cancer	4
Menke-van der Houven van Oordt	2015	EGFR	cetuximab	Colorectal cancer	10
Muyllé	2015	CD20	rituximab	B-cell lymphoma	5
Oosting	2015	VEGF-A	bevacizumab	Renal cell carcinoma	22

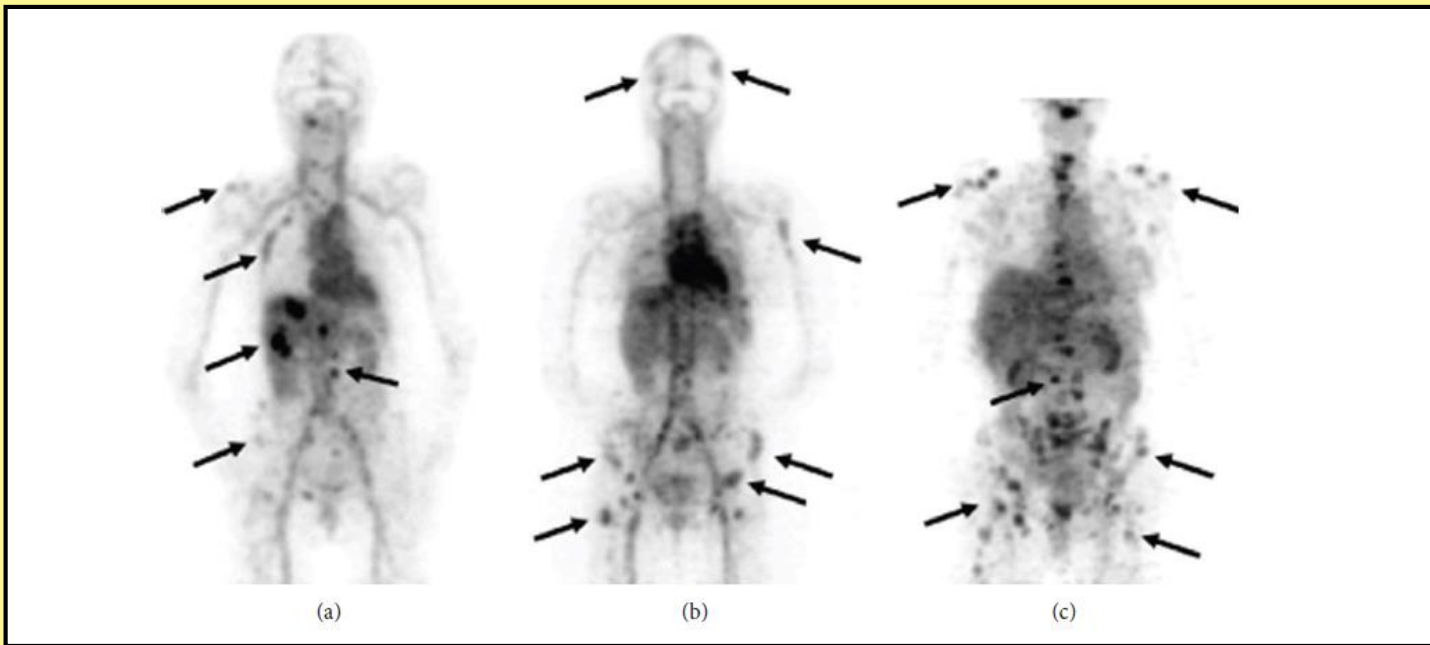
# $^{89}\text{Zr}$ Trastuzumab



In 25 % of invasive breast carcinomas, there is an overexpression of HER2 receptor. Trastuzumab is the inhibitor tumor cell proliferation agent used in pharmacological treatment of breast cancer for the HER2+ overexpressing metastatic breast cancer.

Biological  $t\frac{1}{2}$  over 28d and washout 20w.

# $^{89}\text{Zr}$ Trastuzumab



$^{89}\text{Zr}$ -Trastuzumab uptake 5 days after inj. (a) a patient with liver and bone metastases (b)and (c) two patients with multiple bone metastases. A numbers of lesions haven't see before immunoPET.

This images indicate the potential use of  $^{89}\text{Zr}$ -Trastuzumab to improve the diagnosis of patients with HER2-positive breast cancer especially when lesions are inaccessible for biopsy.

# $^{89}\text{Zr}$ -nanoparticles

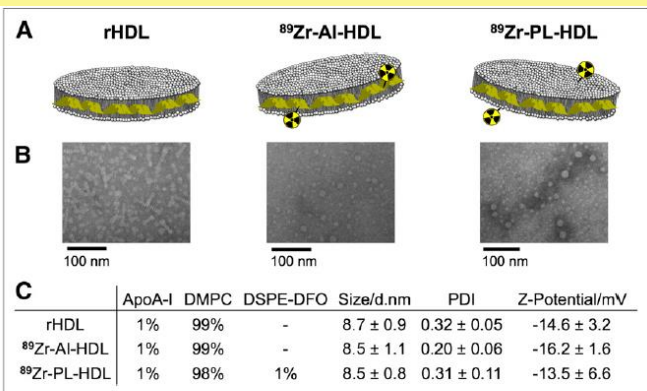
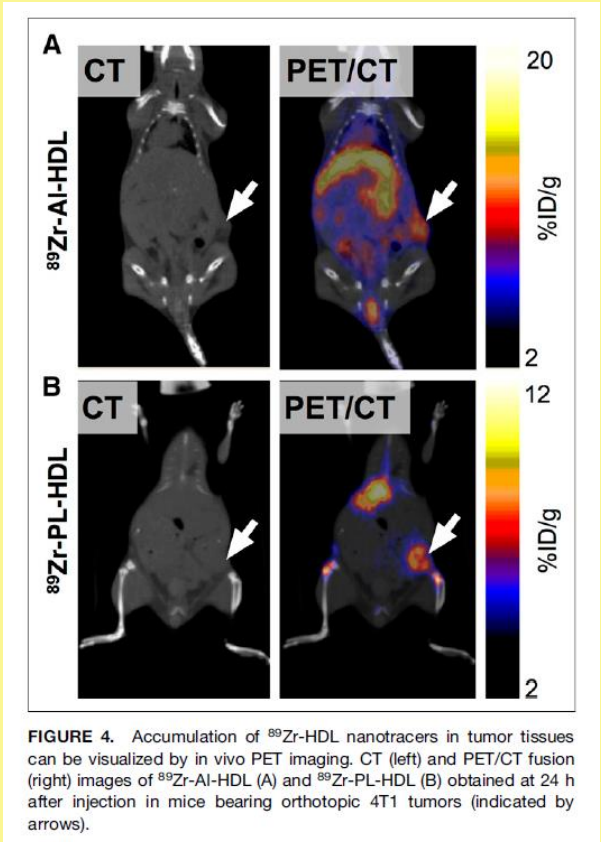


**FIGURE 1.** Structure and composition of rHDL and  $^{89}\text{Zr}$ -HDL nanotracers. (A) Schematic of rHDL (left),  $^{89}\text{Zr}$ -Al-HDL (middle), and  $^{89}\text{Zr}$ -PL-HDL (right). (B) Transmission electron microscopy images of rHDL (left), Zr-Al-HDL (middle), and Zr-PL-HDL (right). (C) Composition (in mol %), size, polydispersity index (PDI), and surface charge of rHDL,  $^{89}\text{Zr}$ -Al-HDL, and  $^{89}\text{Zr}$ -PL-HDL presented as mean  $\pm$  SD ( $n = 3$ ).

plaque, and its specificity for macrophages has been established (16). Furthermore, in 2 recent studies, we have demonstrated its ability to deliver an antiinflammatory drug to macrophages in atherosclerotic plaques with great specificity (17,18). To enable HDL use for quantitative PET imaging of TAMs, we here present the design and synthesis of 2 different  $^{89}\text{Zr}$ -modified reconstituted HDL (rHDL) nanotracers and their in vivo evaluation in an orthotopic mouse model of breast cancer. Specifically, we labeled either its protein component (apolipoprotein A-I [apoA-I]) or its phospholipid load and examined the agent's TAM targeting using in vivo PET imaging and ex vivo analyses, including immunohistochemistry. Additionally, we prepared 2 fluorescent analogs of our radiolabeled  $^{89}\text{Zr}$ -rHDL nanotracers to allow us to gain insight into their cellular targets by flow cytometry.

High-density lipoprotein (I)  
been exploited for MR mol

# Development and Characterization of Clinical-Grade $^{89}\text{Zr}$ -Trastuzumab for HER2/neu ImmunoPET Imaging

## CONCLUSION

The present study showed that clinical-grade  $^{89}\text{Zr}$ -trastuzumab can be manufactured with high stability and maintenance of antigen binding. The first immunoPET radiopharmaceutical displayed excellent tumor accumulation, with high T/NT ratios and a biodistribution similar to that of  $^{111}\text{In}$ -trastuzumab (which was previously used successfully in a clinical study of metastatic breast cancer patients) at a significantly higher spatial resolution and with better T/NT ratios. These data validate this radiopharmaceutical for further clinical testing.

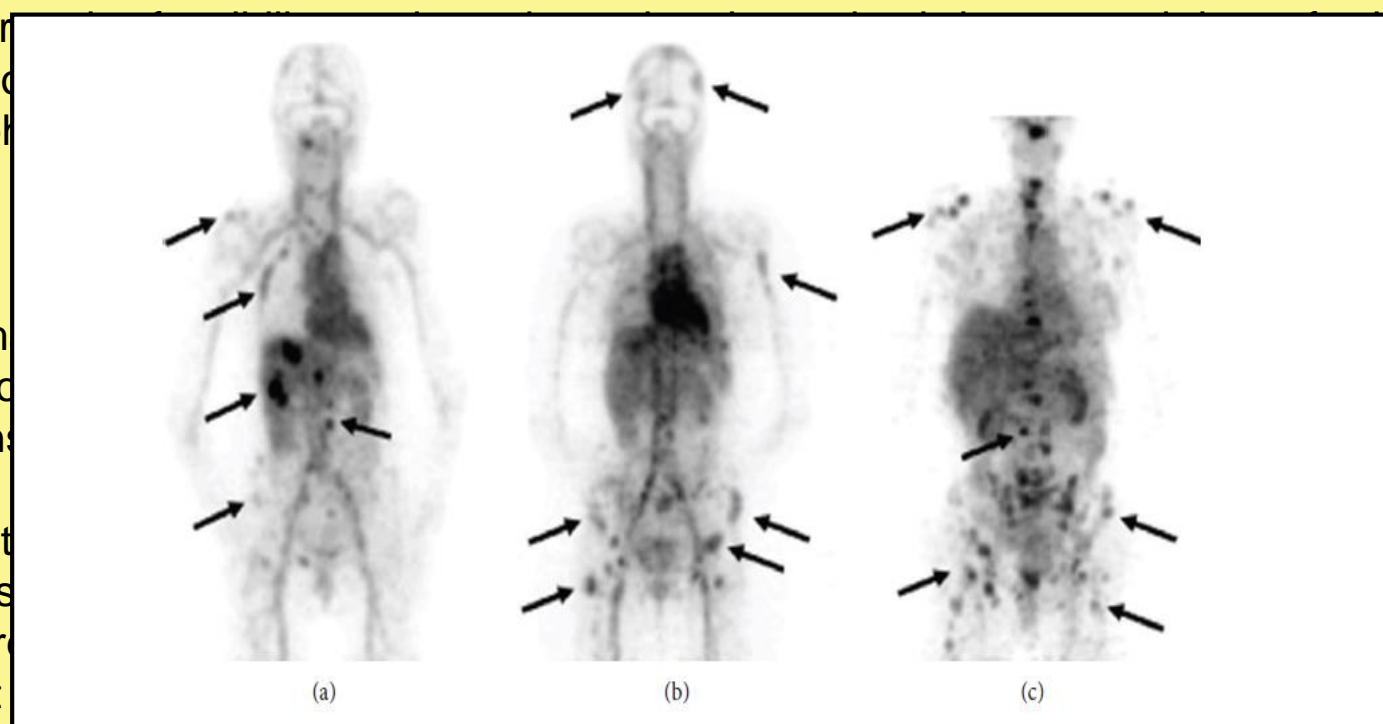
# Biodistribution of $^{89}\text{Zr}$ -trastuzumab and PET Imaging of HER2-Positive Lesions in Patients With Metastatic Breast Cancer

EC Dijkers et al. Clinical Pharmacology & Therapeutics 2010. Volume 87 Number 5, 586593.

We performed the mono-  
tomographic  
lesions.

Fourteen  
trastuzumab  
mg for the  
PET scans.

The results  
by tumors  
patients re-  
treatment



ministration of  
ron emission  
ER2)-positive

sq of  $^{89}\text{Zr}$ -  
-naive and 10  
nt at least two

zumab uptake  
zumab-naive  
trastuzumab  
ions allowed

PET imaging of most of the known lesions and some that had been undetected earlier. The relative uptake values (RUVs) ( $\text{mean} \pm \text{SEM}$ ) were  $12.8 \pm 5.8$ ,  $4.1 \pm 1.6$ , and  $3.5 \pm 4.2$  in liver, bone, and brain lesions, respectively, and  $5.9 \pm 2.4$ ,  $2.8 \pm 0.7$ ,  $4.0 \pm 0.7$ , and  $0.20 \pm 0.1$  in normal liver, spleen, kidneys, and brain tissue, respectively.

PET scanning after administration of  $^{89}\text{Zr}$ -trastuzumab at appropriate doses allows visualization and quantification of uptake in HER2-positive lesions in patients with metastatic breast cancer.

Two serum examination radiography (C mass and bone scan biopsy of on histology mediastinum our hospital means emitting as described intravenous dose 50 i lymph node right side

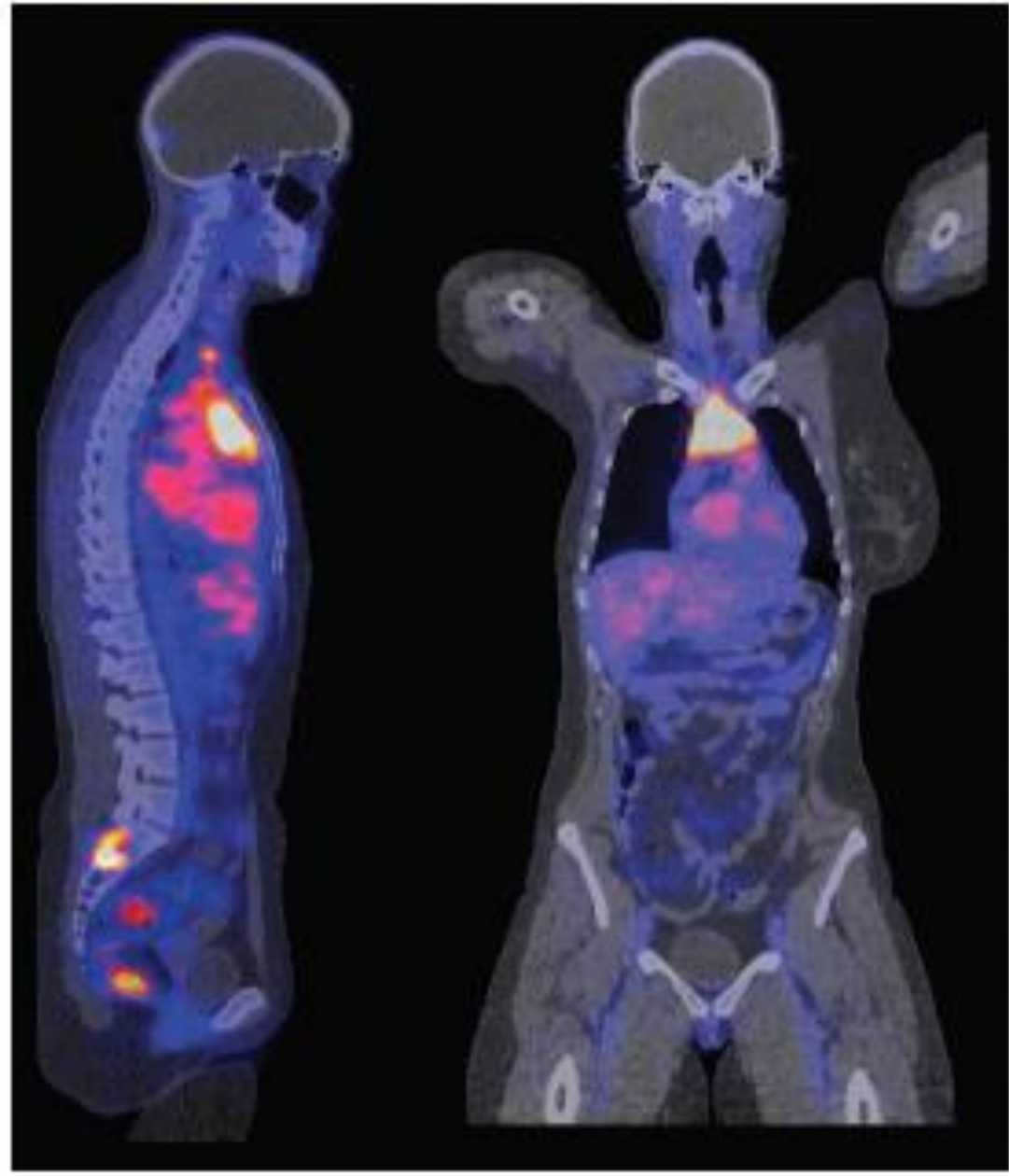


Fig 1.

kup, the Physical tomography - diastinal c it on the - asized, a b nor cells l lesion, a fferred to sively by positron s tried out ays after e (protein - al mass, s 3 on the cted.

## **<sup>89</sup>Zr-trastuzumab and <sup>89</sup>Zr-bevacizumab PET to Evaluate the Effect of the HSP90 Inhibitor NVP-AUY922 in Metastatic Breast Cancer Patients**

Sietske B.M. Gaykema<sup>1</sup>, Carolien P. Schröder<sup>1</sup>, Joanna Vitfell-Rasmussen<sup>5</sup>, Sue Chua<sup>5</sup>, Thijs H. Oude Munnink<sup>1</sup>, Adrienne H. Brouwers<sup>2</sup>, Alfons H.H. Bongaerts<sup>3</sup>, Mikhail Akimov<sup>6,7</sup>, Cristina Fernandez-Ibarra<sup>6,7</sup>, Marjolijn N. Lub-de Hooge<sup>2,4</sup>, Elisabeth G.E. de Vries<sup>1</sup>, Charles Swanton<sup>5</sup>, and Udai Banerji<sup>5</sup>

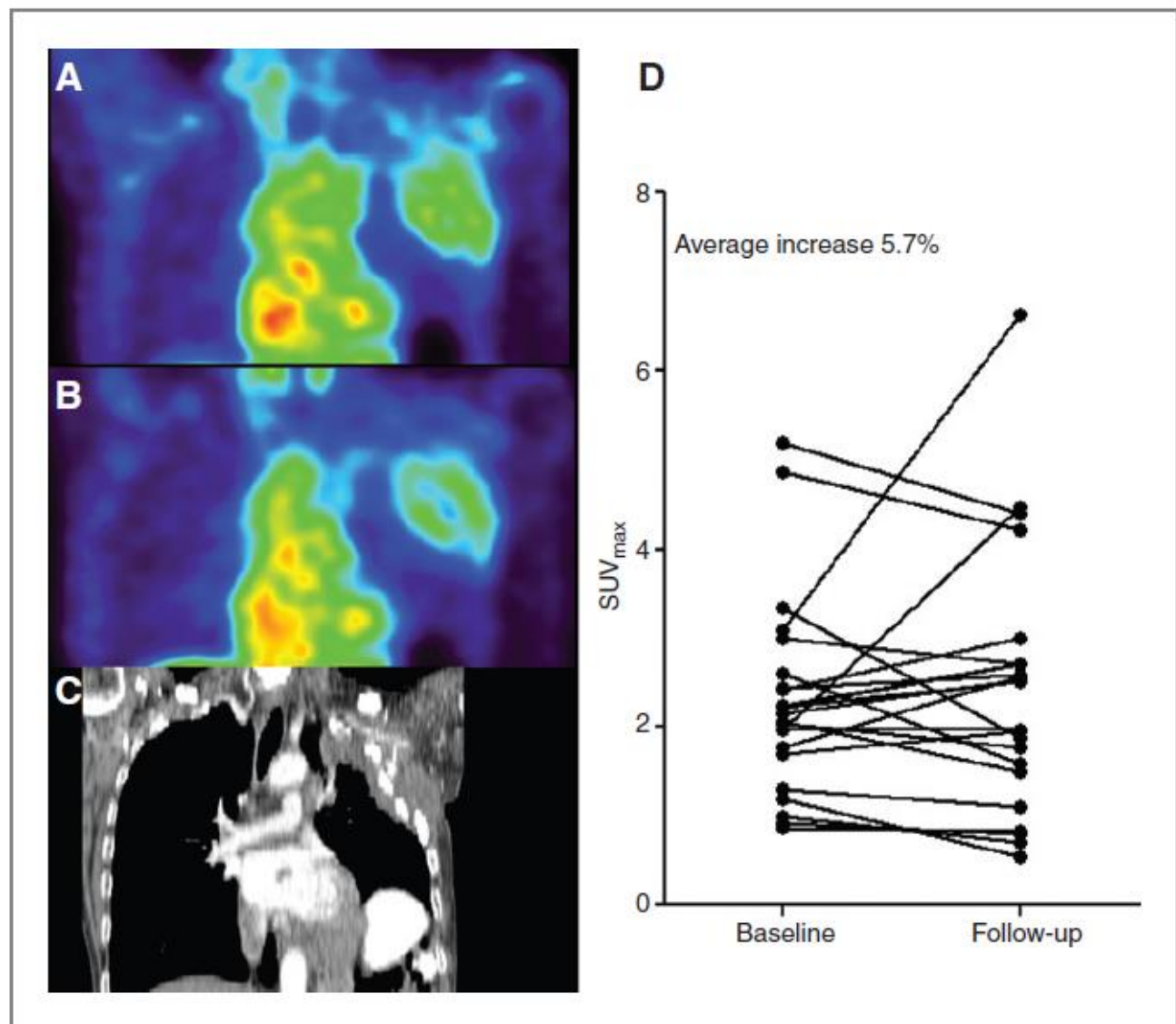
**Purpose:** HSP90 chaperones have key client proteins that are involved in all hallmarks of breast cancer growth and progression. The primary aim of this clinical trial was to evaluate the feasibility of using <sup>89</sup>Zr-trastuzumab PET (for HER2-positive breast cancer) or <sup>89</sup>Zr-bevacizumab PET [for estrogen receptor (ER)-positive breast cancer] to determine *in vivo* degradation of client proteins caused by the novel HSP90 inhibitor NVP-AUY922.

**Experimental Design:** Of note, 70 mg/m<sup>2</sup> NVP-AUY922 was administered intravenously in a weekly schedule to patients with advanced HER2 or ER-positive breast cancer. Biomarker analysis consisted of serial PET imaging with 2[18F]fluoro-2-deoxy-D-glucose (FDG), <sup>89</sup>Zr-trastuzumab, or <sup>89</sup>Zr-bevacizumab. Response evaluation was performed according to RECIST1.0. FDG, <sup>89</sup>Zr-trastuzumab, and <sup>89</sup>Zr-bevacizumab distributions were scored visually and quantitatively by calculating the maximum standardized uptake values (SUV<sub>max</sub>). In blood samples, serial HSP70 levels, extracellular form of HER2 (HER2-ECD), and pharmacokinetic and pharmacodynamic parameters were measured.

**Results:** Sixteen patients (ten HER2-positive and six ER-positive tumors) were included. One partial response was observed; seven patients showed stable disease. SUV<sub>max</sub> change in individual tumor lesions on baseline versus 3 weeks <sup>89</sup>Zr-trastuzumab PET was heterogeneous and related to size change on CT after 8 weeks treatment ( $r^2 = 0.69$ ;  $P = 0.006$ ). Tumor response on <sup>89</sup>Zr-bevacizumab PET and FDG-PET was not correlated with CT response.

**Conclusions:** NVP-AUY922 showed proof-of-concept clinical response in HER2-amplified metastatic breast cancer. Early change on <sup>89</sup>Zr-trastuzumab PET was positively associated with change in size of individual lesions assessed by CT. *Clin Cancer Res*; 20(15); 3945–54. ©2014 AACR.

**Figure 4.** Representative coronal  $^{89}\text{Zr}$ -bevacizumab PET images of a patient scanned before (A) and after (B) 3 weeks of treatment. The patient had a large tumor mass in the chest wall.  $^{89}\text{Zr}$ -bevacizumab PET could be performed in 6 of 10 patients of which 5 underwent repeated scan procedures. The CT scan pretreatment is shown in C. D, a heterogeneous response in individual tumor lesions ( $n = 23$ ) between baseline and follow-up, with an average increase of  $\text{SUV}_{\max}$  of 5.7%.



# Conclusion

- $^{89}\text{Zr}$  Nuclear properties ( $t_{1/2}=78.4\text{h}$ ,  $E\beta^+= 395.5 \text{ kev}$ ) are suitable for immunoPET.
- How to produce  $^{89}\text{Zr}$  from Medical Cyclotron.
- The actual recovery and formulation solution, with the evaluation of the different media used.
  - Overview of  $^{89}\text{Zr}$  ligands and challenge for the future
- $^{89}\text{Zr}$  tracers application state of art and possible future applicaton.